Operando μ-Raman study of the membrane water content in the polymer electrolyte membrane fuel cell: Effects of gas flow-field geometry and temperature

Thi Bich Hue Tran, Patrice Huguet, Arnaud Morin, Mike Robitzer, Stefano Deabate

Operando μ-Raman Measurement of the Water Distribution Along and Across the Membrane in the Fuel Cell

Thi B. H. Tran[1,*], Patrice Huguet[1], Arnaud Morin[2], Mike Robitzer[3], Stefano Deabate[1,z]

[1]IEM, Univ Montpellier, ENSCM, CNRS, Montpellier, France
[2]Université Grenoble Alpes, CEA-Liten, Grenoble F-38000, France
[3]ICGM, Univ Montpellier, ENSCM, CNRS, Montpellier, France

[*]Present address: Université Grenoble Alpes, CEA-Liten, Grenoble F-38000, France

[z]E-mail: stefano.deabate@umontpellier.fr

Abstract

To obtain a fundamental understanding of the transport regimes governing the electrochemical behavior and ageing of the polymer electrolyte membrane fuel cell, the measurement of the membrane in- and through-plane water distribution is essential. In this paper, operando μ-Raman spectroscopy is used to probe the water content of the Nafion® membrane in a model fuel cell working at constant stoichiometry and relative humidity. Water concentration profiles crossing the membrane thickness are obtained with μm resolution at different locations of the active surface: at the middle and close to the inlets/outlets of the reactant gases, at the feed gas channel and under-lands areas. The influence of the operating temperature and of the current density delivered by the cell are investigated. Of particular interest for perspective fuel cells, the membrane inner water partition appears highly heterogeneous when operating at ambient conditions, and dependent on the delivered current. The increase of temperature decreases the membrane water content at all the probed positions and induces a less uneven water distribution. The membrane hydration appears to be a key parameter for understanding the water redistribution between cathode and anode with the change of the cell operating conditions.

Introduction

Fuel cells (FC) represent a highly efficiency energy conversion technology. Combined with dihydrogen fuel, a clean energy carrier, the polymer electrolyte membrane fuel cell (PEMFC) technology has a great potential to reduce both carbon dioxide emissions and dependence on fossil fuels. Thus, PEMFCs are currently regarded as strategic products by major industrial countries.[1,2] Nevertheless, two main interrelated technical challenges delay PEMFC large-scale marketing: cost and durability.[3-5] Consequently, improving water and heat management arises as a major factor.[6-8]

The water distribution within the electrochemical system results from the interplay between in- and through-plane fluxes. The in-plane water transfer is mainly governed by the flow of the reactant gases and liquid water accumulation along the distribution channel. Simultaneously, water is redistributed by the membrane between the opposite electrodes, via coupled mass and charge transport processes involving both H_2O and H^+ species: mainly back-diffusion and electroosmosis. The significance of other contributions, e.g. convective or thermoosmotic, remains under debate.[6]

The occurring of coupled transport phenomena and mechanisms, together with the complexity of the FC design (consisting in a layered structure of media with different porosity and permeability), results in heterogeneous through- and in-plane conditions concurrently affecting temperature, current, concentration and pressure of reactants and water. Accordingly, the way the FC performs and degrades is also inhomogeneous, difficult to predict and manage.

The development of suitable models of the PEMFC electrochemical behavior, performances and ageing requires the fundamental understanding of the different transport mechanisms and, therefore, the detailed knowledge of the through-plane water distribution across the different components of the membrane-electrode assembly (MEA). The polymer membrane, placed at the middle of the electrochemical system and separating the electrodes, appears as the keystone of the 3D water distribution and represents an example of the typical back-coupling of transport phenomena which confers particular complexity to the water distribution issue. Indeed, the membrane permeability to water depends on the membrane water content and the last depends, in turn, on the external water concentration as it is determined by the in- and through-plane fluxes. Further, the water sorption ability of the membrane presumably depends on the different, local environmental conditions inside the FC: typically, the uneven constriction occurring at the scale of the alternating gas distribution channels and lands for the current collection, hindering the homogeneous swelling of the membrane and locally altering the porosity of the active (ALs) and gas diffusion layers (GDLs). The information of the local water content in the membrane during operation is, then, a critical issue for the validation of mass transfer models, the definition of optimized operating conditions and the development of efficient systems with innovative designs for efficient water management. A consequent research effort has been carried out on the development of operando techniques able to probe the water content and partition in the membrane.[7,9,10] Among these, operando Raman microspectroscopy has been developed more recently by a limited number of research groups.[11-20] Operando μ-Raman is a laboratory-scale, sensitive and selective technique based on the accumulation of Raman spectra across the membrane thickness. Once the raw signal is properly corrected for the different optical and spectroscopic aberrations, the concentration profile of the water crossing the membrane is obtained with both in- and through-plane μm spatial resolution. More details about the principle of operando μ-Raman and depth-profiling measurements through perfluorosulfonic polymers can be found in Deabate et al..[17]

In our previous article,[20] we reported the evolution of the membrane hydration at the middle of the active surface as a function of the FC operating temperature and delivered current. The work here reported completes and goes further. Water concentration profiles are collected close to the inlets and outlets of the reactant gases, at locations corresponding to the gas feed channel and to the lands for the current collection, at operating temperatures ranging from ambient conditions to 80°C. In order to progress in the understanding of limiting phenomena occurring under the dry operating conditions currently envisaged and relationships with water transfers across the MEA, the cell is operated at low relative humidity (20% RH) and high flows of the reactant gases. Results allow to map the uneven water partition both in- and trough-plane and attest the crosswise relationships between the water distribution, the current delivered by the cell and the FC operating temperature.

Experimental

Cell. The model cell used for operando μ-Raman measurements is the same used in Tran et al.[20] and consists of stainless steel monopolar plates with a single serpentine gas distribution channel (active area 4 cm^2, channel width and depth 1 and 0.5 mm respectively, lands width 1.2 mm) coated by a gold layer (10 μm thick) improving electrical contact and preventing steel corrosion. To provide the access of the Raman exciting irradiation to the membrane, the upper plate (cathode side) is drilled at the center (1 mm hole). A round cover glass and a compressible gasket squeezed by a tightening ring ensure the tightness. Four distinct cathode BPs are used, differing for the position of the hole which is placed either at the gas distribution channel or at the land for the current collection, at the middle of the active surface or close to the inlets/outlets of the gaseous reactives (Figure 1).

Materials and Assembly. Nafion® N115 membrane (thickness ~ 125 μm at 50% RH, EW = 1100 g mol^{-1}) from DuPont De Nemours is used as received. Electrodes are Johnson Matthey on Toray paper TGP-H-060 (thickness 190 μm, 0.4 mg cm^{-2} Pt). To provide the access of the Raman exciting irradiation to the membrane, GDL and AL are removed over a circular surface (Ø400 μm) as previously reported.[20] The cell is finally clamped with a tightening torque of 5 Nm and placed at 120°C during 1 hour.

FC Operating Conditions. The PEM fuel cell is operated with pure oxygen and hydrogen at atmospheric pressure. The input and output conditions (gases temperature, pressure, flow rate and humidity) are managed and monitored by a home-made test bench. RH is measured by a Rotronic HygroPalm capacitive sensor. The cell temperature is managed by a Pt 100 probe placed at the cathode plate. The reactants are supplied at the same temperature as the cell, in counter-flow arrangement (anode and cathode channels face each other across the membrane and respective flows have opposite directions), at constant RH (20% at both inlets) and stoichiometry (25/100 for H_2/O_2 respectively). The high flow rates are needed to avoid water condensation in the channel and at the optical window (the last representing a cold point).

The electrochemical management of the cell is carried out by a Biologic SP-150 potentiostat equipped with a VMP3 booster. The FC polarization curves are established point by point using constant current chronopotentiometry. The impedance of the cell is measured at each point by electrochemical impedance spectroscopy (EIS) (current perturbation 10 mA, frequency range 2×10^{-1} to 5×105 Hz).

Previous to Raman measurements, the PEMFC is operated during at least 30min, until to attain steady conditions of voltage, ohmic resistance and outlet gas RH.

Mass Balance Measurements. Parameters regarding the water mass balance measurement, i.e. gas flow rates supplied at the electrodes, RH, pressure at the inlet and outlet and cell temperature, are recorded continuously during experiments. The amount of water (D / mol s^{-1}) incoming and outgoing each electrode is calculated for each operating condition. The extra water flow (J / mol s^{-1} cm^{-2}), which corresponds to the molar flow rate of water from the electrochemical reaction, is:

$$J_{\text{extra water}} = (D_{\text{water}}^{\text{outlet}} - D_{\text{water}}^{\text{inlet}})/S_{\text{active}} \quad (1)$$

where $D_{\text{water}}^{\text{outlet}}$ and $D_{\text{water}}^{\text{inlet}}$ are the molar flow rates of water at the outlet and inlet, respectively, and S_{active} is the cell active area (S / cm^2). The ratios between the extra water measured at each electrode by the RH probes and the overall flow related to the whole water produced by

the electrochemical reaction, i.e. calculated from the current delivered by the FC, are:

$$R^{\text{cathode}} = J^{\text{cathode}}_{\text{extra water}}/J^{\text{tot}}_{\text{extra water}} \quad (2)$$

$$R^{\text{anode}} = J^{\text{anode}}_{\text{extra water}}/J^{\text{tot}}_{\text{extra water}} \quad (3)$$

It follows that:

$$R^{\text{tot}} = R^{\text{cathode}} + R^{\text{anode}} = (J^{\text{cathode}}_{\text{extra water}} + J^{\text{anode}}_{\text{extra water}})/J^{\text{tot}}_{\text{extra water}} \quad (4)$$

Since $J^{\text{cathode}}_{\text{extra water}}$ and $J^{\text{anode}}_{\text{extra water}}$ correspond to experimental values from the RH measurements, while $J^{\text{tot}}_{\text{extra water}}$ is calculated from the current delivered by the cell, R^{tot} is expected to be equal to 1 when the FC operates at the steady state.

Raman Measurements. The PEMFC is placed on an automatic sliding plate and depth-resolved measurements are carried out across the membrane thickness with a step of 1 μm (Figure S1). The experimental in-depth resolution is 7±1 μm.[17] The experimental volume probed at a given position is ≤ 14 μm^3. The collection time for a single spectrum is limited to 1 s to avoid local warming and ~ 220 spectra are cumulated at different positions across the membrane thickness for a single cartography. To ensure high statistics, 15 cartographies are carried out for each experiment and their average performed.

Raman spectra are excited with a 647.1 nm irradiation generated by an Ar–Kr laser. The laser power at the membrane surface is 20 mW. The back-scattered radiation is recovered by a 50X Fluotar objective (maintained at 30°C to avoid damage) and transmitted to a LABRAM1B confocal Raman spectrometer (Jobin-Yvon S.A., Horiba, France) equipped with a charge coupled device detector with a 300 grooves mm-1 grating and cooled by a double Peltier effect. The water volume fraction Φ_V and hydration number λ of the membrane are calculated at each probed position from the ratio between the intensities of the ν(O–H) mode and some selected Raman bands belonging to the ionomer chemical groups, as detailed elsewhere.[17,20,21] The so-obtained sorption isotherms of the Nafion® 115 membrane, attesting the reliability and sensitivity of the method, are reported in Figure S2.

The water concentration-profiles obtained by depth-resolved Raman measurements are affected by artificial gradients and poor resolution. Actual water profiles are then recovered by the geometrical correction of spherical aberrations and by a convolution procedure using the instrumental spreading function, according to the procedure detailed in Deabate et al..[17] After treatment of the raw data, the depth-resolution of the μ-Raman measurement is assumed to correspond to ~ 1 μm (probed volume ~ 1 μm^3).

Results and Discussion

Figure 2 reports representative polarization curves of the model PEMFC operated at different T (T_{room} corresponding to around 25°C) and related ohmic resistances. Results are very similar to those previously reported[20] and attest the reproducibility of measurements obtained with the different BPs. Since operating conditions, cell design and materials are not optimized for efficiency but for *operando* microspectroscopy and for enhancing limiting phenomena related to low RH operation, the electrochemical performances of the model FC are lower than the state-of-the-art. It should therefore be pointed out that performances do not affect neither the nature of the water transport phenomena involved nor their relationships with the FC electrochemical behavior, so that results obtained here can be used for the better

understanding of state-of-the-art cells.

The FC performance increases with T (Figure 2a), which corresponds to the general decrease of the integral ohmic resistance (Figure 2b), the last attributable (as a first approximation) to the simultaneous enhancing of proton mobility in the ionomer phase (of both the electrodes and the membrane), reactive gases diffusion and catalyst activity. Concurrently, ohmic losses are also affected by the current density j delivered by the FC. At T ≤ 50°C, the cell resistance appears to increases with the increase of j. At 80°C, resistance initially drops and then stay unaffected. This last behavior has already been reported under similar operating conditions and attributed either to lack of temperature management (i.e. resistance values are recorded before the temperature stabilization)[22] or to lacking membrane hydration when using low hydrated dioxygen at low current densities.[23] Neither hypotheses can be applied here since steady conditions have been carefully checked and μ-Raman measurements attest no significant changes of the membrane water content with j at this temperature (*vide infra*). As discussed in the following, the particular behavior of the ohmic resistance observed at 80°C (and, to a lesser extent at 50°C) can be attributed to the evolution with j of the water amount transferred from the cathode across the membrane and hydrating the anode ionomer phase.

Figures 3 and 4 show the evolution with current of the water concentration gradients crossing the membrane in the PEMFC operating at T_{room} and 80°C, respectively. The behavior observed at the intermediate T is in-between these two extreme cases (see Figures S3 and S4). All water concentration profiles are practically linear, attesting that the value of the water diffusion coefficient does not vary significantly along the membrane thickness for a given T and j. Confirming our previous results,[18,20] the membrane average water content decreases with the increase of T (Figure 5). When the cell is operated at $T \leq 50$°C, the membrane hydration also depends on the applied current density: it first increases at the FC start up and then decreases with j. The last results allow to explain the general increase of the FC resistance with j (Figure 2b). On the whole, the most hydrated position corresponds to the middle of the active area and the lower the cathode inlet/anode outlet (see also Figure S5). The highest water content is observed at the anode channel (Φ_V = 0.133 at 25 mA cm^{-2} and T_{room}) but, overall, the membrane appears more hydrated under the lands for the current collection than at the channel. It should be noted that the hydration difference at the lands/channel scale was yet observed by μ-Raman in a FC with parallel channels but, in that case, the phenomenon was largely more enhanced.[20] The discrepancy between the water contents at the under-lands and channel positions increases with the increase of j, which strongly suggests the accumulation of water from the electrochemical reaction at the lands because of simultaneous less effective drainage by gases and more effective heat evacuation by lands. A further, concomitant reason could be the fact that the channel has been identified as the area hosting the larger local currents,[24,25] therefore subjected to higher local warming inducing lower actual RH.

The membrane water loss with T was previously attributed to the relative amount of water produced by the electrochemically reaction becoming negligible compared to that injected via the reactants hydration when the cell T increases: the water activity of the gases at the inlets staying invariant, the actual RH inside the cell decreases.[20] Indeed, the maximum values measured at T_{room} for the RH at the cathode and anode outlets are 65% and 45% respectively, while both stay very close to 20 % at 80°C. The membrane dehydration with j was also previously reported[18,20] and mainly ascribed to the spontaneous increase of the FC inner T due

to the increase of electrochemical heat and ohmic losses, with a lesser contribution from to the increase of pressure drops due to the increase of the gas reactants flows with current (inducing the decreasing of the actual amount of water injected in the cell). The observation that the membrane water content becomes unaffected by j at T = 80°C agrees with the consistent decrease of the ohmic losses due to the enhanced proton mobility at this temperature (which implies the lower spontaneous warming of the cell for a given increase of j) and to the concomitant lower impact of any T increase on the actual RH (because of the higher water saturation pressure). Results here reported agree with EIS measurements and definitively confirm what was previously hypothesized,[18,20] namely that the membrane dehydration phenomena observed with the increase of T and j do not concern only the middle of the active surface but equally involve the whole membrane volume.

Membrane inner water gradients ($\Delta\Phi_V/d$ where $\Delta\Phi_V = \Phi_{V\,/\,\text{cathode}} - \Phi_{V\,/\,\text{anode}}$ and d is the membrane thickness as measured by μ-Raman, see Figures S6 and S7) are observed whatever the probed position and the operating conditions, even if strongly affected by all the investigated parameters. Data show that: (i) at $T \leq 50$°C, the inlet and outlet positions (referring to the cathode) show opposite gradients (particularly at the lower j), which should correspond to the occurrence of diffusion water fluxes in opposite direction at these locations as expected for the counter-flow configuration; (ii) gradients measured at the middle of the active surface and, to a lesser extent, at the under-lands outlet position exhibit intermediate behavior i.e. initially directed from the anode to the cathode, the gradient progressively reverses with the increase of j (which strongly suggests the inversion with the current increase of the external water gradient and, consequently, water fluxes crossing the membrane); (iii) on the whole, gradients are largest at the inlets/outlets positions than at the center (but this difference becomes negligible with the increase of both T and j); (iv) on the whole, gradients are slightly less marked at the under-lands than at the channel area (for a given location at the active surface); (v) but for the under-lands position at the cathode outlet at T_{room} and T = 32°C, gradients decrease with the increase of both T and j. At T = 80°C, the behavior of the weak gradients remaining becomes completely erratic.

As far as self- or low-humidified PEMFC are concerned, experimental and theoretical studies have so far considered the water concentration gradient at the membrane always oriented from the cathode to the anode, independently from the direction of the net water flux (see Feindel et al.[26] and references therein). Then, a main result here is to show that inner gradients (and so, diffusion fluxes which most often represent the main contribution) can exhibit opposite direction depending on the position at the active surface and can reverse as the current delivered by the FC varies.

The decrease of the membrane inner water gradient with T reflects the decrease of the external gradient, i.e. the difference between the gaseous water activities at the anode and cathode sides of the cell. This is due to both (i) the fact that the amount of the water produced by the electrochemical reaction at the cathode becomes progressively less weighty compared to that injected into the cell by hydration of the reactants and (ii) the increase of the MEA (particularly the membrane) permeability with T,[27] enhancing water flows due to back-diffusion. Water mass balance measurements reported in Figure 6 clearly show that, even if the gaseous water activity measured at the FC cathode outlet stays always larger (as expected) for all the temperature and current conditions, the transfer of water from the electrochemical

reaction to the anode increases with T.

The decrease of the membrane inner water gradient with j (observed for the most of the probed positions) is related to the larger dehydration of the membrane anode side (initially more hydrated) compared to the cathode for a given current increase (see Figure 3, S3 and S4). In principle, assuming that the spontaneous warming of the cell with j should equally affect both sides of the membrane (at least at the macroscopic scale), increasing j at a given T should correspond to the increase of the external water gradient. In spite of this, the concomitant decrease of the membrane permeability due to dehydration (as attested by μ-Raman measurements), hindering water transfer to the cathode, and enhancing of the eletroosmosis flows with j (also reinforced by the increase of the electroosmotic drag coefficient with the membrane water loss[28]) induce the membrane anodic side to dehydrate more rapidly.

The different evolutions with j of the water transfer across the MEA observed at different T (Figure 6) result then from the interplay between the antagonistic effects of temperature and current on the net through-plane water flux and their relationships with the membrane water content. At the lower T (T_{room} and 32°C), when the membrane hydration changes considerably with j (i.e. decreases), water transfer from the cathode to the anode decreases continuously with the current increase, which attest the global loss of the membrane permeability, overwhelming any effect due to the spontaneous warming of the cell. Differently, at the operating T = 50°C and more particularly 80°C, when the membrane hydration stays almost unaffected by current, water transfer from the cathode to the anode first increases with j, presumably because of the increase of the external gradient, and then decreases with the prevailing of the electroosmosis flow over back-diffusion. Since, at the maximum current, $R^{cathode} = 1$ at the lower T while remaining < 0.8 at the higher T, these results suggest that a better water removal from the cathode by transfer through the membrane to the anode should be included among the different phenomena improving the FC performance with the increase of the operating T. $U_{iR\text{-corrected}}$ reported in Figure 2c confirms that, at 80°C, losses at low j mainly originates from the electrodes, presumably because of lower actual local RH.

The μm resolution of the depth-resolved measurements allows access to the water content of the membrane surface i.e. to compare the membrane hydration behavior at the opposite sides. Figure 7 represents the water distribution at the anode and cathode membrane surfaces as a function of the FC operating T and j (according to data reported in Figure S5, the evolution of the water content between two next probed positions being assumed as continuous). Both surfaces exhibit unevenly water content at the channel-land scale as well as along the inlet to outlet direction but, as long as $T \leq 50$°C, the heterogeneity of the water distributions at the opposite sides is completely different. This attest the complexity of the interplay between the different water transport mechanisms (diffusion, electroosmosis and convection), FC design (serpentine configuration of the channels) and operation conditions (counter-flow feeding). At T_{room}, the membrane cathode side, directly exposed to water from the electrochemical reaction, exhibits gradual water accumulation from the inlet to the outlet, with the driest area corresponding to the channel inlet (where water evacuation by gas is more effective) while identical water concentrations are observed at the outlet channel and under-land positions. Somehow unexpected, the cathode side appears globally less hydrated than the anode. Differently from the cathode, but as usually expected for the FC fed counter-flow, the anode side shows higher water accumulation at the middle of the active surface, particularly at the

channel. The inlet and outlet areas exhibit very similar water contents, with the channel as the less hydrated position. The increase of both *T* and *j* dehydrates both sides of the membrane to very similar water contents and decreases all differences between channel and ribs, inlets and outlets until an almost homogeneous water distribution is attained at 80°C, close to the membrane hydration state observed at the equilibrium at 20% *RH*.

Of interest for PEMFC intended to operate at ambient conditions, the coupling of macro- and microscopic measurements allows to characterize the evolution of the actual feed gases *RH* along the flow path as a function of the cell operating conditions. Figure 8 reports the example of the *RH* evolution at the FC cathode and anode sides as a function of the delivered *j,* at *T* = 32°C. Values at the ends of the channels (full symbols) correspond to the direct measurements of the water activity by the *RH* probe while the others (open symbols) are deduced from the water content of the membrane surface according to μ-Raman i.e. water contents are converted into *RH* values using the sorption isotherm reported in Figure S2 and assuming the membrane surface at the equilibrium with the gas phase. At the cathode side, the water activity always increases from the inlet to the outlet, almost linearly at low *j* but with a larger water accumulation close to the end of the flow path when the current increase (a larger spread between macro- and microscopic measurements is observed at this area). The water vapor concentration distribution along the anode is more strongly affected by *j*. At low current, the water activity first increases from the inlet to exceed values measured at the cathode and reach the maximum at the midstream area, presumably owing to the strong back-diffusion from the highly wetted cathode at this position. Then, moving to the downstream region, water concentration decreases due to the forward diffusion to the drier cathode and larger electroosmosis (the last increasing because of the lower average water content of the membrane at this area[28]) but always remaining larger than at the cathode. Thus, at the lower *j*, the anode side appears to have larger *RH* along most part of the flow path. The opposite is observed at larger currents. With the increasing of *j*, the position where anode and cathode show the same water activity moves progressively from the cathode outlet/anode inlet region towards the opposite side. The global value of the water activity decreases at both sides but more rapidly at the anode channel. At the largest *j*, the *RH* stays homogeneous and very close to 20% along the anode flow path (despite the larger water transfer from the cathode, Figure 6) while increases suddenly at the cathode downstream area.

Conclusions

Raman microspectroscopy has been applied to improve the knowledge of the steady-state water distributions occurring in the PEMFC under a range of operating temperatures. This work, even if mainly representing a phenomenological description of the Nafion hydration behavior under specific operating conditions, highlights aspects of the water content distribution which could hardly have been anticipated by modeling. This points out the concern of *operando* investigation to address the actual behavior of perfluorosulfonic materials and produce useful inputs for forthcoming numerical studies.

As far as low *T* are concerned (which, together with low humidity represents the operating conditions targeted for automotive applications), results attest the highly heterogeneous in- and through-plane water distribution inside the membrane, and this despite the high flow rates used in this work. The membrane hydration, strongly dependent on both the operating temperature

and the current delivered by the FC, in turn affects (together with *T*) the flows redistributing gaseous water between the cathode and anode compartments of the cell. This implies that the effective modeling of through-plane water fluxes requires the accurate knowledge of the local water content of the membrane.

At low *T*, two different water distribution are observed at the opposite surfaces of the membrane. Hydration at the cathode side is governed by the accumulation of the electrochemically produced water along the flow path. Water distribution at the anode results from the counter-flow management of gaseous reactants and exhibits larger water concentration at the midstream area.

Under the specific operating conditions concerning this work, i.e. constant stoichiometry and *RH*, the increase of both FC temperature and current dehydrates both sides of the membrane to almost identical and homogeneous water contents. This implies that the effect of current on the water distribution becomes negligible when the cell is operated at the standard $T = 80°C$.

Globally, the FC performances appear to strongly depend on two main properties of the membrane: ohmic resistance (strictly related to the water content) and water permeability, the last governing the adequate removal of water from the cathode and, thus, probably ensuring the better hydration of the electrodes ionomer phase. The evolution of both resistance and permeability with *j* affects concomitantly the cell electrochemical behavior up to the operating $T = 50°C$. At $T = 80°C$, the FC performances are no longer dependent from the membrane hydration, the last staying unaffected by current, and the membrane ability to transfer water from the cathode to the anode becomes the main parameter affecting performances at low *j*.

Forthcoming *operando* μ-Raman studies will be devoted, on the one hand, to extend our investigation to further operating conditions affecting mass transport losses (e.g. cell compression, land/channel size and design, weak stoichiometry…) and, on the other, to improve experimental conditions and cell design as to investigate state-of-art MEA.

References

1. G. Morrison, J. Stevens and F. Joseck, *Transport. Res. C Emerg. Technol.*, **87**, 183 (2018).
2. J. Shin, W.-S. Hwang and H. Choi, *Technol. Forecast Soc.*, **143**, 239 (2019).
3. A. de Frank Bruijn and G. J. M. Janssen , in *Fuel Cells*, K.-D. Kreuer, Editor, p. 249, Springer, New York (2013).
4. T. Wilberforce, Z. El-Hassan, F. N. Khatib, A. Al Makky, A. Baroutaji, J. G. Carton and A. G. Olabi, *Int. J. Hydrogen Energy*, **42**, 25695 (2017).
5. Fuel Cell System Cost – 2017, Doe Hydrogen and Fuel Cells Program Record, can be found under www.hydrogen.energy.gov/pdfs/17007_fuel_cell_system_cost_2017.pdf, 2017.
6. K. Jiao and X. Li, *Prog. Energy Combust. Sci.*, **37**, 221 (2011).
7. S. Deabate, G. Gebel, P. Huguet, A. Morin and G. Pourcelly, *Energy Environ. Sci.*, **5**, 8824 (2012).
8. Z. Yang, Q. Du, Z. Jia, C. Yang and K. Jiao, *Energy*, **183**, 462 (2019).
9. A. Bazylak, *Int. J. Hydrog. Energy*, **34**, 3845 (2009).
10. Q. Meyer, Y. Zeng and C. Zhao, *Adv. Mater.*, **31**, 1901900 (2019).
11. P. Huguet, A. Morin, G. Gebel, S. Deabate, A. K. Sutor and Z. Peng, *Electrochem. Comm.*, **13**, 418 (2011).

12. Y. Tabuchi, R. Ito, S. Tsushima and S. Hirai, *J. Power Sources*, **196**, 652 (2011).
13. M. Hara, J. Inukai, K. Miyatake, H. Uchida and M. Watanabe, *Electrochim. Acta*, **58**, 449 (2011).
14. M. Hara, J. Inukai, B. Bae, T. Hoshi, K. Miyatake, M. Uchida, H. Uchida and M. Watanabe, *Electrochim. Acta*, **82**, 277 (2012).
15. A. Martinelli, C. Iojoiu and N. Sergent, *Fuel Cells*, **12**, 169 (2012).
16. A. Z. Peng, A. Morin, P. Huguet, Y. Lanteri and S. Deabate*, Phys. Chem. Chem. Phys.*, **16**, 20941 (2014).
17. S. Deabate, P. Huguet, G. Gebel, Y. Lanteri, Z. Peng and A. K. Sutor, *Fuel Cells*, **14**, 677 (2014).
18. Z. Peng, V. Badets, P. Huguet, A. Morin, P. Schott, T. B. H. Tran, M. Porozhnyy, V. Nikonenko and S. Deabate, *J. Power Sources*, **356**, 200 (2017).
19. H. Nishiyama, S. Takamuku, K. Katsuhiko, S. Lacher, A. Iiyama and J. Inukai, *J. Phys. Chem. C*, **124**, 9703 (2020).
20. T. B. H. Tran, P. Huguet, A. Morin, M. Robitzer and S. Deabate, *Electrochim. Acta*, **372**, 137904 (2021).
21. Z. Peng, P. Huguet, S. Deabat, A. Morin and A.-K. Sutor, *J. Raman Spectrosc.*, **44**, 321 (2013).
22. F. N. Büchi and G. G. Scherer, *J. Electroanal. Chem.*, **404**, 37 (1996).
23. B. Andreus, *Solid State Ion.*, 2004, *168*, 311.
24. M. Reum, S. A. Freunberger, A. Wokaum and F. N. Büchi *J. Electrochem. Soc.*, **156**, B301 (2009).
25. M. Reum, A. Wokaum and F. N. Büchi, *J. Electrochem. Soc.*, **156**, B1225 (2009).
26. K. W. Feindel, S. H. Bergens and R. E. Wasylishen, *J. Am. Chem. Soc.*, **128**, 14192 (2006).
27. F. N. Büchi and S. Srinivasan, *J. Electrochem. Soc.*, **144**, 2767 (1997).
28. Z. Peng, A. Morin, P. Huguet, P. Schott and J. Pauchet, *J. Phys. Chem. B*, **115**, 12835 (2011).

Figures

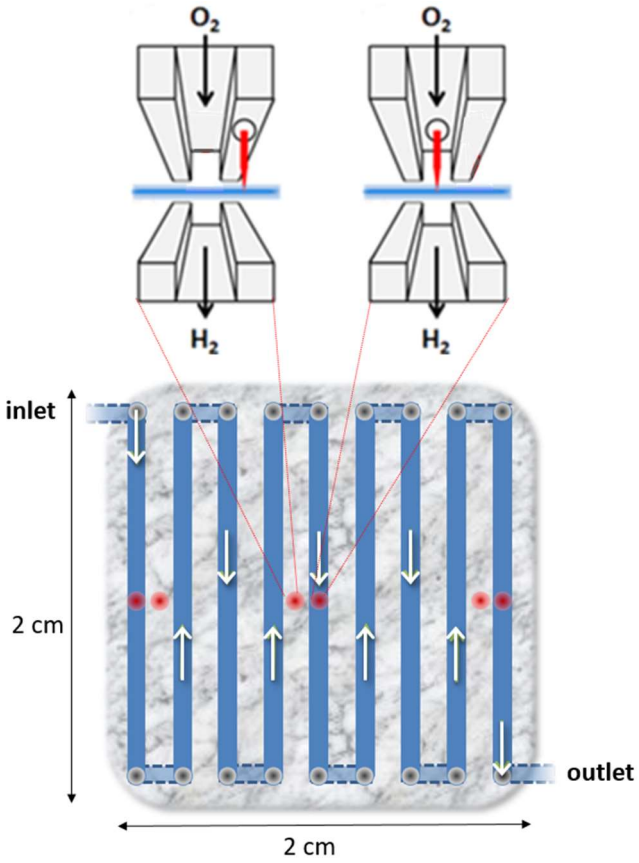

Figure 1. In scale schematic representation of the configuration of the gas distribution channel and positions probed by the Raman exciting irradiation.

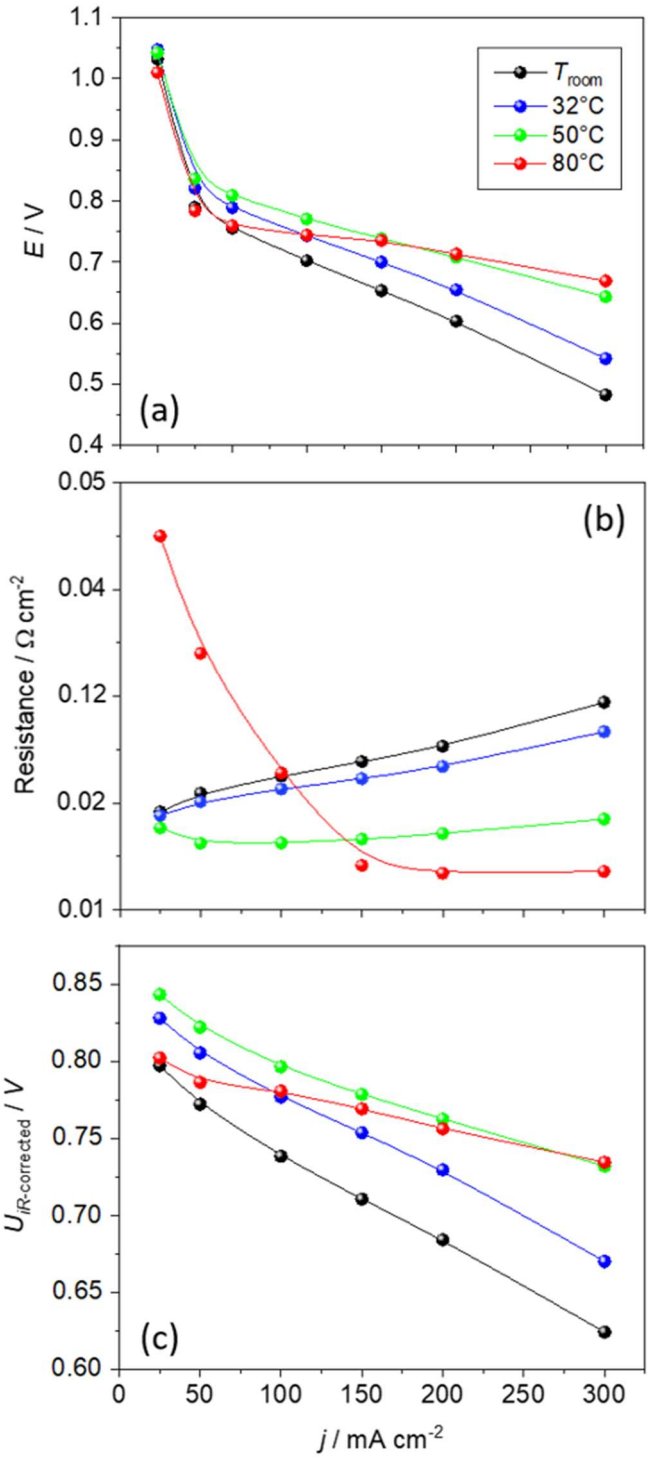

Figure 2. (a) FC polarization curves at different operating *T* (reported in the legend) and corresponding evolutions of (b) the ohmic resistance and (c) the *iR* corrected potential as a function of the delivered current.

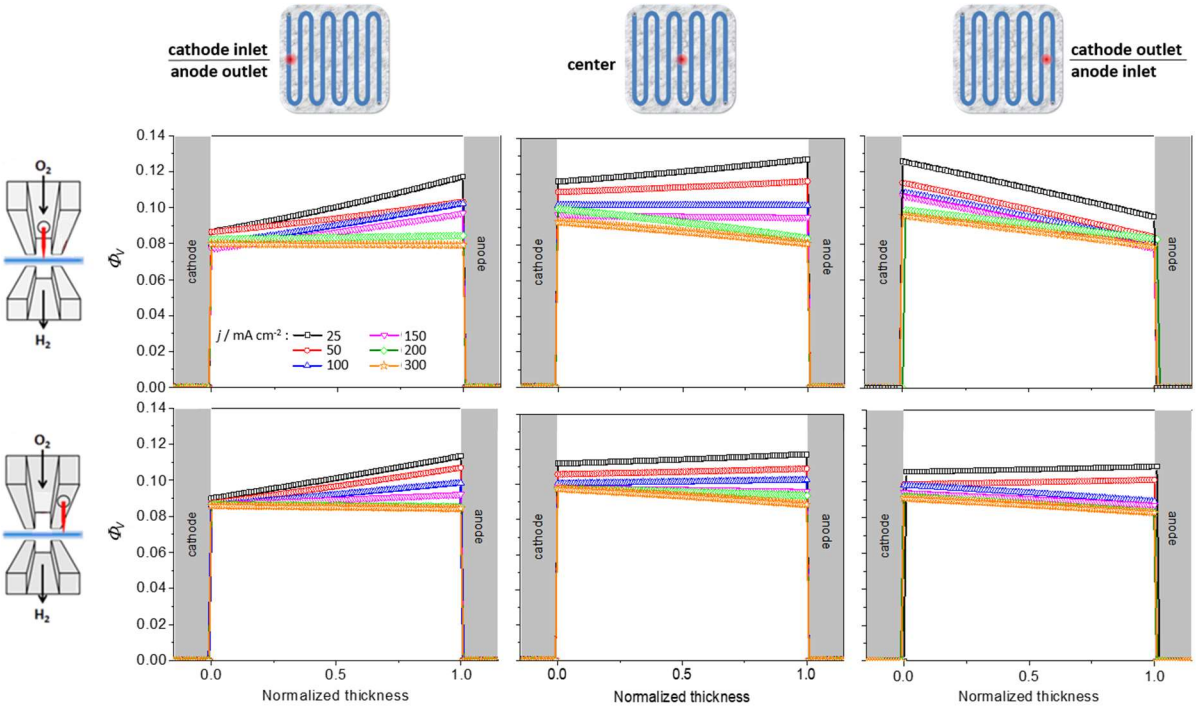

Figure 3. Comparison of the evolution of the membrane inner water distribution with the current density (reported in the legend) at the different probed position (top: channel, bottom: lands, left: cathode inlet, middle: center, right: cathode outlet) in the cell operated at T_{room}.

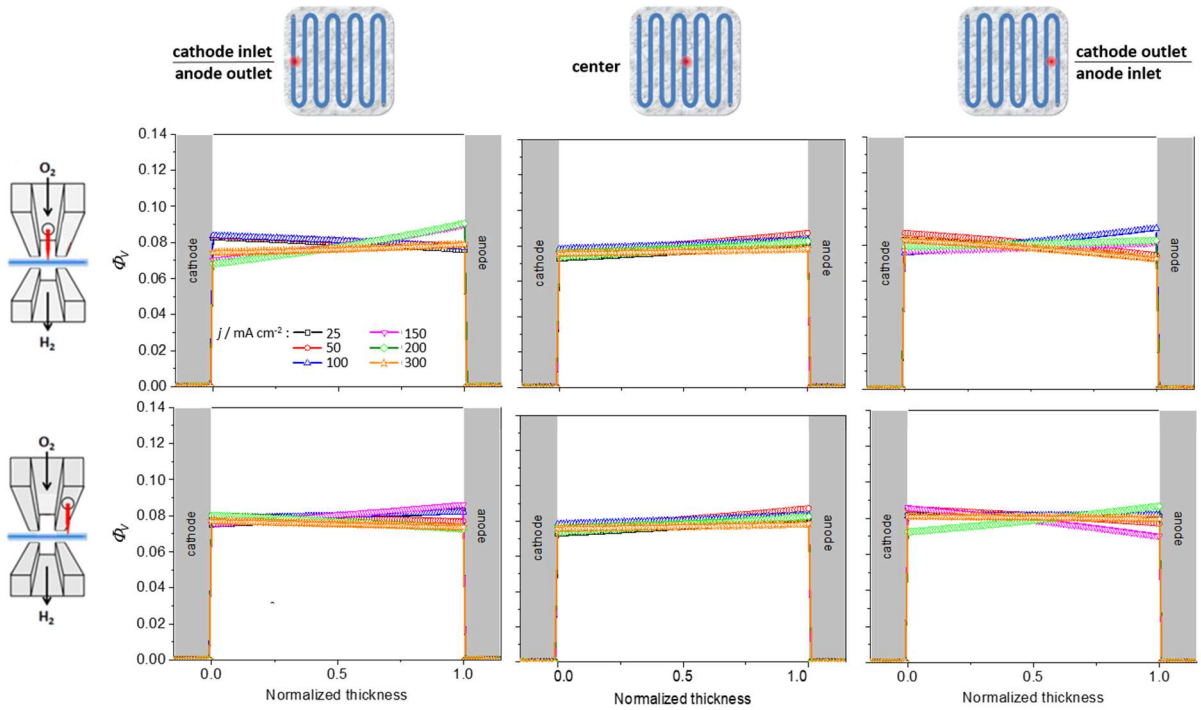

Figure 4. Comparison of the evolution of the membrane inner water distribution with the current density (reported in the legend) at the different probed position (top: channel, bottom: lands, left: cathode inlet, middle: center, right: cathode outlet) in the cell operated at 80°C.

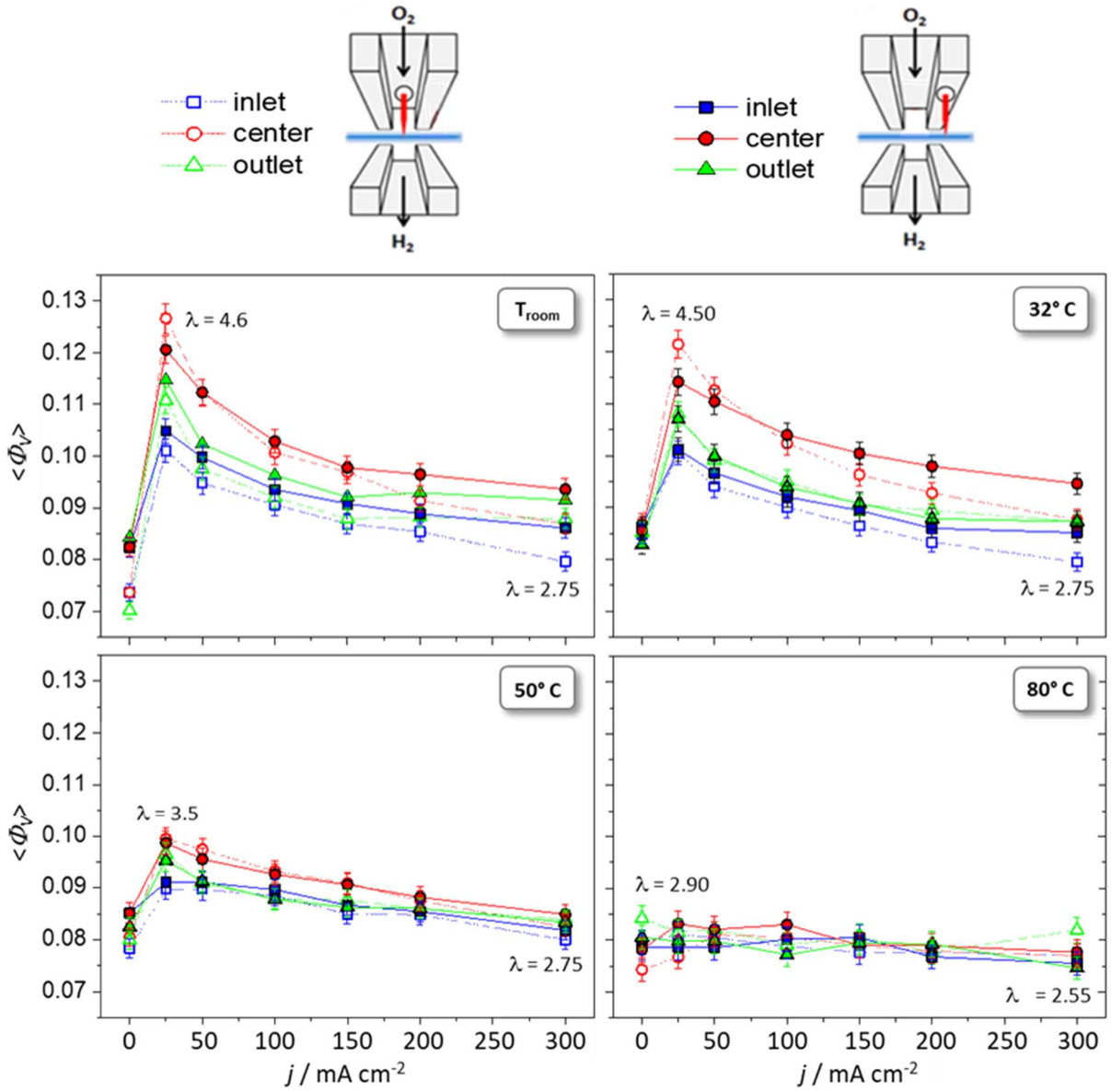

Figure 5. Evolution with the current density of the membrane average water volume fraction at the channel (open symbols) and under-lands (full symbols) positions in the cell operated at different *T*. The minimum and maximum water contents measured for a given *T* are also reported as hydration number $\lambda = [H_2O]/[SO_3]$.

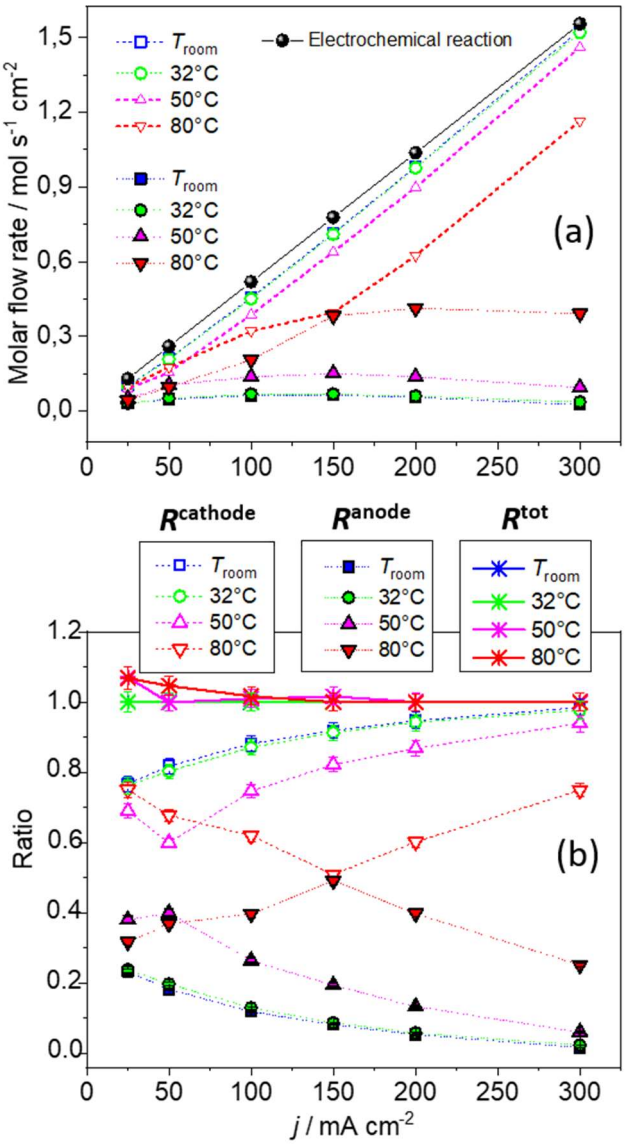

Figure 6. (a) Evolution with current of the extra water flows measured at the cathode (open symbols) and anode (full symbols) sides (the evolution of the overall flow of the electrochemically produced water is also reported in full black symbol; errors are inside the symbol size) and of (b) the ratios between the extra water flow measured at each electrode and the overall extra water, at the different FC operating *T* (reported in the legend).

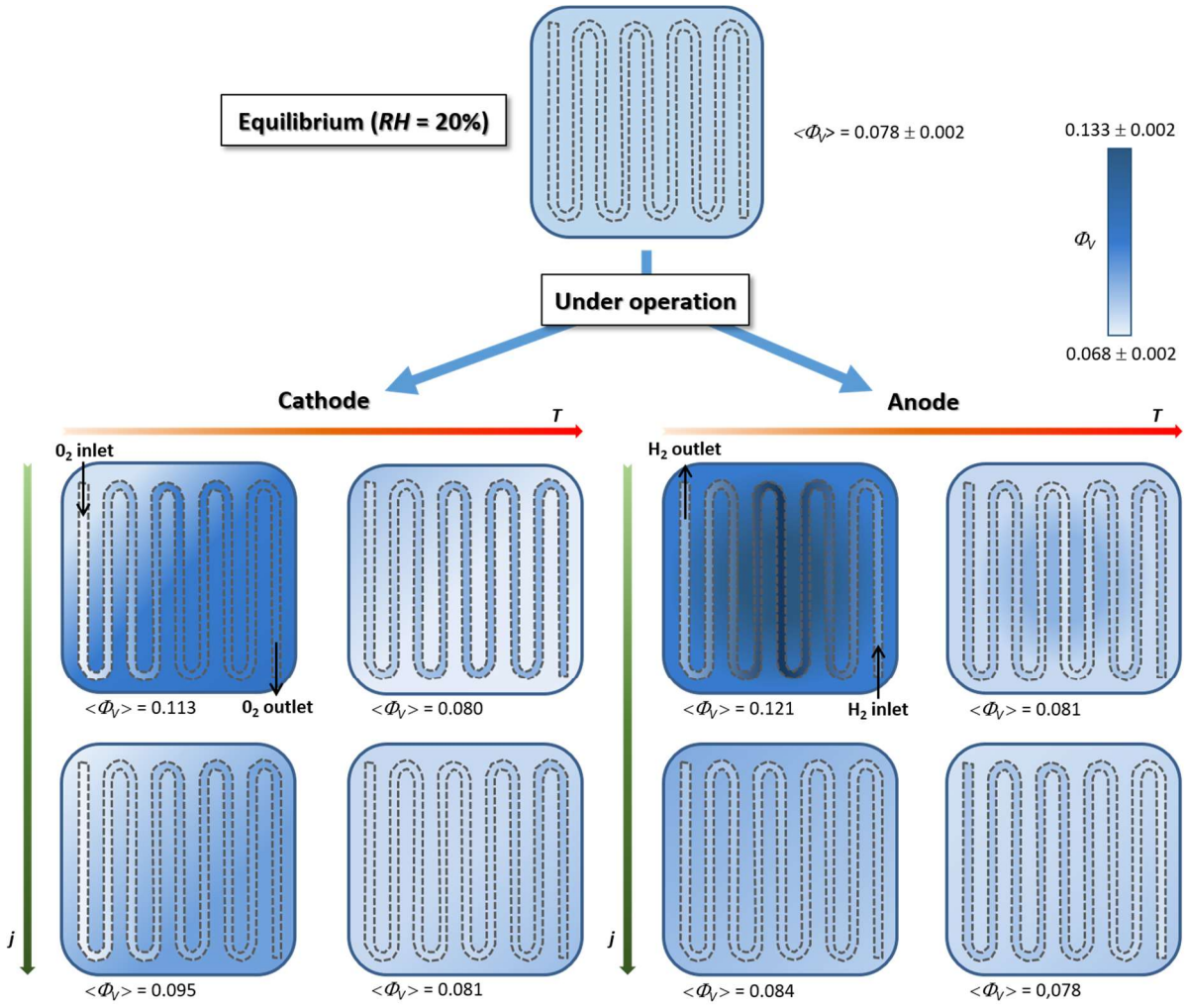

Figure 7. Schematic representation of the water distribution at the anode and cathode membrane surfaces and the effects of the FC operating T and delivered j.

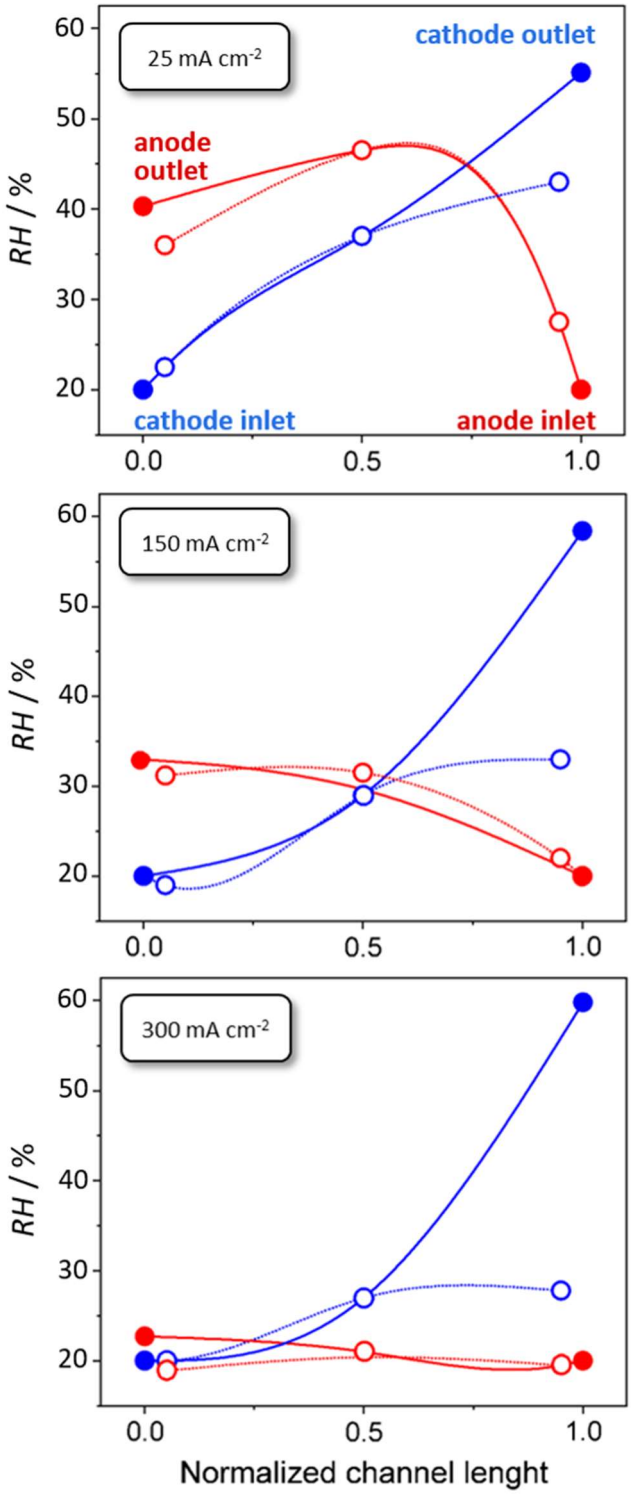

Figure 8. Evolution of the *RH* distribution along the anode (red) and cathode (blue) gas flow paths with the current density (reported in the legend) in the FC operated at T = 32°C. Full symbols correspond to direct measurements at the FC inlets and outlets whereas open symbols are *RH* values deduced from the membrane surface water content as given by μ-Raman.